

Characterization of a Tunable Flattened-Pass-band Fiber Comb Filter

Yong Wook Lee^{1,2} and Jaehoon Jung^{3*}

¹*School of Electrical Engineering, Pukyong National University, Busan 48513, Korea*

²*Interdisciplinary Program of Biomedical Mechanical & Electrical Engineering,
Pukyong National University, Busan 48513, Korea*

³*Department of Electronics and Electrical Engineering, Dankook University, Yongin 16890, Korea*

(Received December 27, 2018 : revised March 19, 2019 : accepted September 19, 2019)

The optical characteristics of a tunable flattened-pass-band fiber comb filter, based on the polarization-diversified loop configuration, are investigated using the Poincaré-sphere representation. In the design process, the spectral flatness is checked quantitatively, and the tunability of the pass band is demonstrated experimentally. Theoretical calculations show that the filter also exhibits desirable dispersion and polarization properties. The orientation angles of rotatable wave plates for the wavelength tunability of the filter are obtained. Furthermore, we elaborate on the multiple angle loci produced by degeneracies through the combination of optical elements within the loop of the filter.

Keywords : Tunable wavelength filter, Polarization insensitive

OCIS codes : (060.2420) Fibers, polarization-maintaining; (060.2310) Fiber optics; (230.7408) Wavelength filtering devices; (260.5430) Polarization

I. INTRODUCTION

Optical-fiber comb filters have attracted considerable attention for a wide variety of applications in multiwavelength optical systems, such as dense-wavelength-division-multiplexing (DWDM) systems, multiwavelength laser sources, and nonlinear optical switching devices [1-6]. They serve as essential components, due to their capability of selecting desired signals and isolating adjacent signals.

To improve the flexibility of optical comb filters, various approaches to implement continuous wavelength tunability have been proposed, using Sagnac birefringence filters (SBFs) based on birefringence combination [7-12], a double-loop Mach-Zehnder interferometer (MZI) [4, 13, 14], or a fiber Bragg grating [15, 16]. In particular, extensive investigations on comb filters using the polarization-diversified loop configuration (PDLC) have been carried out, due to their ability to switch or continuously tune the pass bands. The authors have proposed zeroth-order tunable comb filters using a section of polarization-maintaining fiber (PMF) [17, 18] and first-order Solc and Lyot comb filters using [19, 20]

two sections of PMF based on PDLC, respectively.

Recently, a continuously tunable polarization-independent pass-band-flattened fiber comb consisting of two sections of PMF was proposed and demonstrated experimentally [21]. The filter transmission and orientation-angle sets of wave plates for wavelength tuning were derived through Jones-matrix formulations. The relationship between wavelength tuning and the final state of polarization (SOP) within the PDLC was also discussed. The arbitrary wavelength tunability in the transmission spectrum was verified by theoretical investigation and experimental results. However, an exact analytic expression for a flat-top transmittance function is required to obtain the wave plate's orientation angles for its continuous wavelength tuning. Besides, the other optical properties of the filter have not been investigated thoroughly.

In this paper, we investigate the characteristics of the tunable pass-band-flattened fiber comb filter. The operating principles of the filter are described, and the orientation-angle loci of the wave plates for wavelength tuning are obtained by the use of the Poincaré sphere. The algorithms for pass-band-shape design and wavelength tuning are presented

*Corresponding author: andyjung@dku.edu, ORCID 0000-0003-4397-7631

Color versions of one or more of the figures in this paper are available online.



This is an Open Access article distributed under the terms of the Creative Commons Attribution Non-Commercial License (<http://creativecommons.org/licenses/by-nc/4.0/>) which permits unrestricted non-commercial use, distribution, and reproduction in any medium, provided the original work is properly cited.

in detail. The multiple orientation-angle sets of the wave plates are derived using a geometrical method via the Poincaré sphere. The optical characteristics are also analyzed, including group-velocity dispersion and differential group delay (DGD).

II. POLARIZATION EVOLUTION WITHIN THE PDLC

Figure 1 shows the schematic of the tunable filter based on the PDLC, which consists of a PBS and two birefringent groups of an HWP, a QWP, and a section of PMF, designated as HWP1, QWP1, and PMF1 in the first group and HWP2, QWP2, and PMF2 in the second group. We denote the PBS's horizontal and vertical axes as the x axis and y axis respectively. The orientation angle of each optical element is defined as the angle between its slow axis and the x axis. Arbitrarily polarized light incident from the IN port might have x - and y -axis components, which are separated by the PBS. The x component travels in the clockwise (CW) direction, while the y component moves in the counterclockwise (CCW) direction in the PDLC. PMF2 is butt-coupled to the PBS so that the slow axis of PMF2 is oriented at 22.5° with respect to the x axis.

In fiber comb filters based on the PDLC, the filter

spectrum is generated by the wavelength-dependent phase retardation $\Gamma = 2\pi BL/\lambda$ between two orthogonal principal states of polarization of the PMF, where B , L , and λ are the birefringence, length of the PMF, and wavelength of light in vacuum respectively. The birefringence and length of both PMFs are 4.166×10^{-4} and 7.2 m respectively, leading to a channel spacing of 0.8 nm.

Generally, a birefringent element allows a point-of-input SOP (s_1, s_2, s_3) on the Poincaré sphere to be rotated by its phase retardation CCW (looking from its slow axis to its fast axis) around the axis, passing its two eigenpolarization states in the Poincaré-sphere representation [22]. We concentrate our attention here on the x component of the light's polarization vector, since the optical characteristics can be investigated simply by analyzing the SOP evolution of light traveling CW within the PDLC [22]. The input SOP is x -polarized and represented by a point $(1,0,0)$ on the Poincaré sphere, and will be converted into a linear polarization with azimuthal angle of $4\theta_{h1}$ by HWP1. If we assume the wave plates to be achromatic, their output SOPs of broadband light will be identical. After passing HWP1, light passes through QWP1, and its output SOP can be obtained by rotating the SOP around the $2\theta_{q1}$ axis CCW by an angle of $\pi/2$. PMF1 moves the SOPs by Γ , which is dependent on wavelength, and the output SOPs become a circle centered on the point with an azimuthal

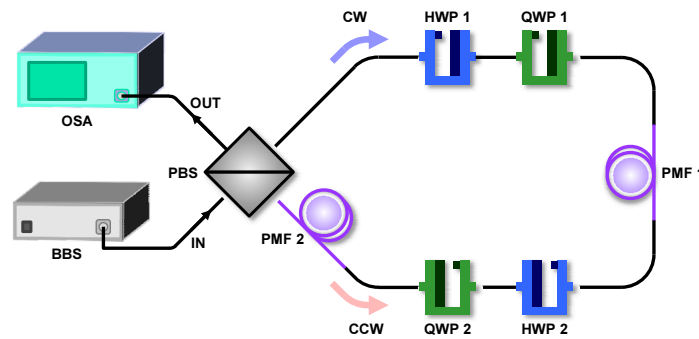


FIG. 1. Schematic diagram of the PDLC.

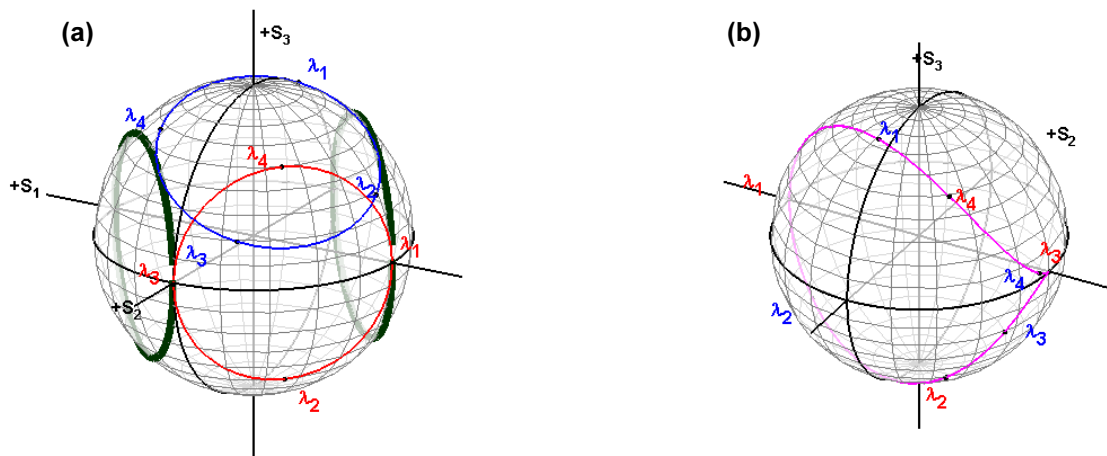


FIG. 2. SOP loci (a) before and (b) after PMF2. The phase shifts in the transmittance correspond to 0° (red) and 45° (blue) respectively.

angle of $2\theta_{PMF1}$ on the equator, with a radius of the distance between the SOP after QWP1 and the center of the circle. Hence, the broadband light source is dispersed into a circular locus by rotation about the axis lying on the equator with longitude $2\theta_{PMF1}$, and the locus is rotated by successive HWP2 and QWP2 before PMF2, while remaining circular in shape over the FSR.

For convenience, we designate 1548.0, 1548.2, 1548.4, and 1548.6 nm as λ_1 , λ_2 , λ_3 , and λ_4 , and their corresponding phase retardations of the PMF as Γ_1 , Γ_2 , Γ_3 , and Γ_4 , respectively. First let us consider the angle combination that produces a transmission spectrum with dip wavelength λ_1 . The SOP loci before PMF2 are shown with transmittance phase shift of 0° (red) and 45° (blue) in Fig. 2(a). The red

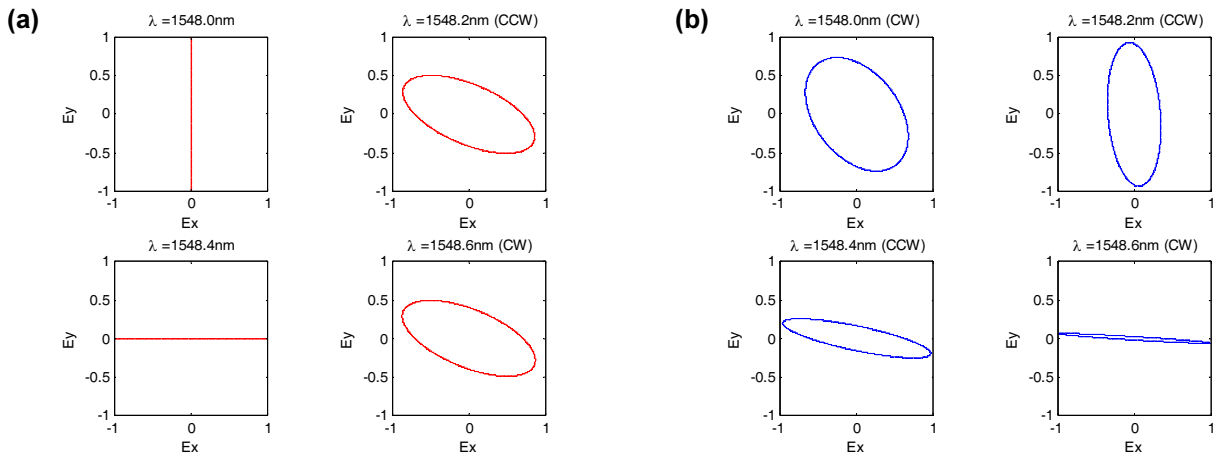


FIG. 3. Polarization ellipses of light traveling CW within the PDLC after PMF2, for phase shifts of (a) 0° and (b) 45° , at λ_1 , λ_2 , λ_3 , and λ_4 .

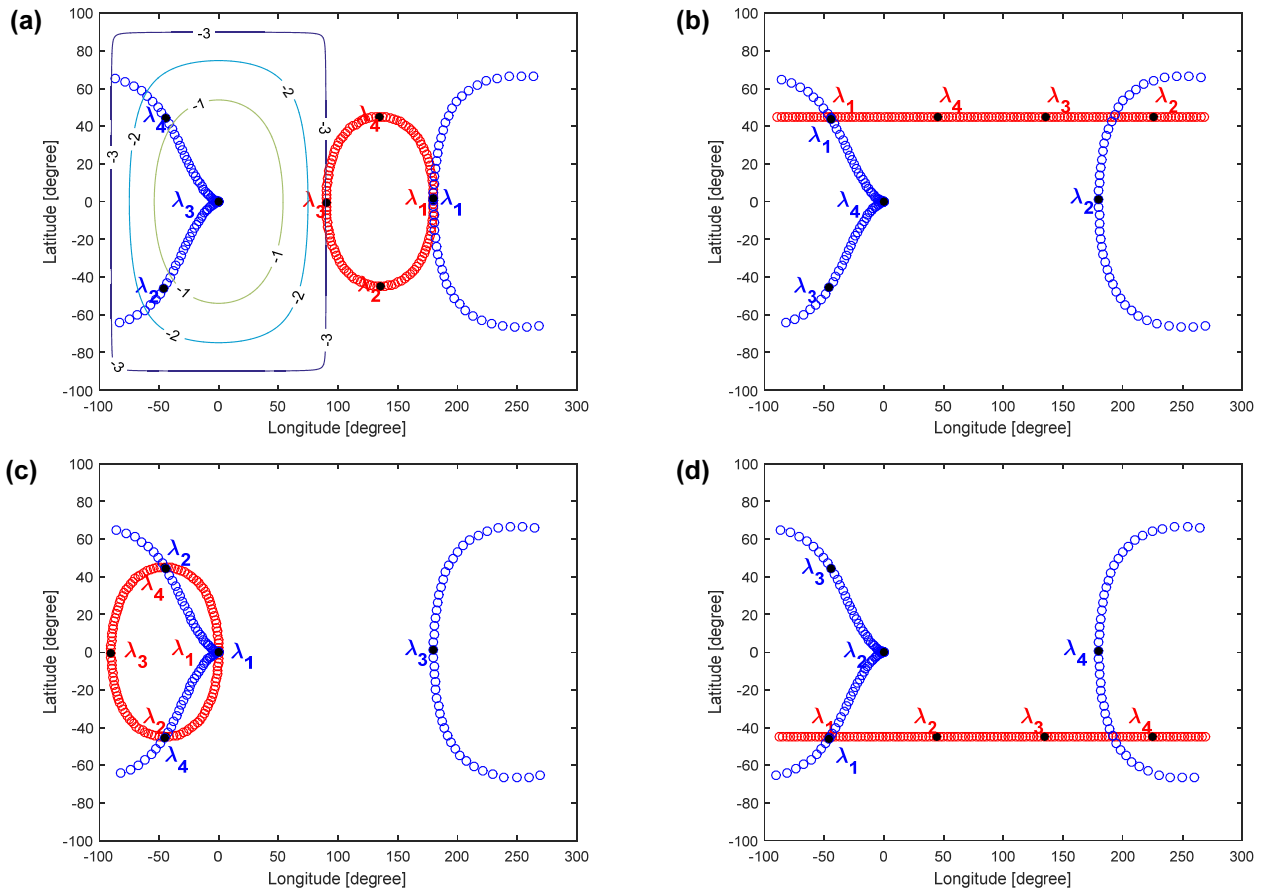


FIG. 4. SOP loci before (blue) and after (red) PMF2, in a world-map description, for phase shifts of (a) 0° , (b) 90° , (c) 180° , and (d) 270° .

circular locus represents the SOP for dip wavelength λ_1 before PMF2. The SOP of λ_1 remains unmoved, while that of λ_3 moves toward (1,0,0) after PMF2, which correspond to the center wavelengths of the stop band and pass band respectively. For a 0.1-nm shift ($\Delta\Gamma=45^\circ$), the circle is rotated around the $2\theta_{PMF1}=45^\circ$ axis tightly between two green circles, and spins at the same time CCW by 45° , becoming the blue circle shown in Fig. 2(a). Thus the SOP of 1548.1 nm ($=(\lambda_1+\lambda_2)/2$), which is located simultaneously on the blue and green circles, will move to (-1,0,0) through rotation by 45° CW, and will be extinguished at the output port. Two circular loci (red and blue) are further dispersed after PMF2, but the final loci are the same in shape but different in wavelength location, implying wavelength tuning. The wavelength locations are those at phase shift 0° (red) and 45° (blue) in Fig. 2(b).

The corresponding final polarization ellipses after PMF2 at the individual wavelengths of light shown in Fig. 2(b) are shown in Figs. 3(a) and 3(b) for the two cases 0° and 45° respectively.

To see the tunability and flat pass band clearly, the SOP loci before (red circles) and after PMF2 (blue circles) of light traveling CW within the PDLC are replotted as world maps in Figs. 4(a), 4(b), 4(c), and 4(d), where the center wavelength of the stop band corresponds to λ_1 , λ_2 , λ_3 , and λ_4 respectively. The SOP loci after PMF2 are identical in shape but different in wavelength location, leading to wavelength tunability of the filter. From the isocontours of transmission shown in Fig. 4(a), it is obvious that the 2-dB bandwidth is larger than 0.4 nm, since $\Delta\lambda = \lambda_4 - \lambda_2 = 0.4$ nm.

To clearly observe continuous wavelength tunability of the filter, the orientation-angle sets of four rotatable wave plates (θ_{h1} , θ_{q1} , θ_{h2} , θ_{q2}) for individual center wavelength λ_p of the pass band are investigated using the method explained above for $\theta_{p1}=0^\circ$. The loci of (θ_{h1} , θ_{q1}) and (θ_{h1} , θ_{h2}) are shown in Figs. 5(a) and 5(b) respectively. The tuning over the FSR is implemented for the angle ranges $-16.4^\circ \leq \theta_{h1} \leq 16.4^\circ$, $67.5^\circ \leq \theta_{q1} \leq 112.5^\circ$, and $-56.2^\circ \leq \theta_{h2} \leq 34.1^\circ$ respectively. The projection of (θ_{h1} , θ_{q1} , θ_{h2} , θ_{q2}) onto

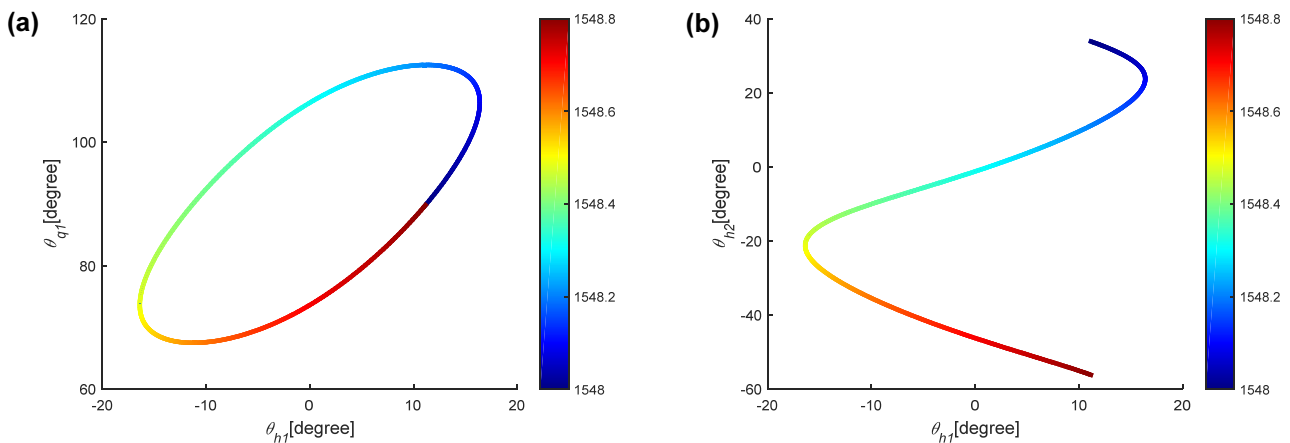


FIG. 5. The orientation-angle loci of the wave plates as a function of dip wavelength: (a) (θ_{h1} , θ_{q1}) and (b) (θ_{h1} , θ_{h2}). These angles are obtained for a dip wavelength increasing from 1548.0 nm to 1548.8 nm over an FSR with a step of 0.005 nm, with θ_{p1} set to 0° .

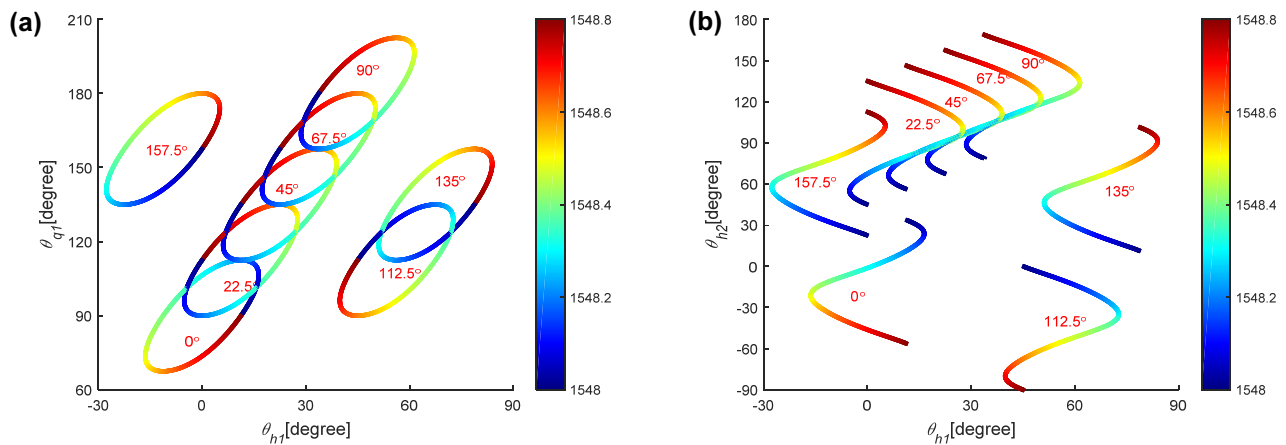


FIG. 6. Wave-plate angle loci of (a) (θ_{h1} , θ_{q1}) and (b) (θ_{h1} , θ_{h2}), for various values of θ_{p1} . The loci are obtained for a dip wavelength increasing from 1548.0 nm to 1548.8 nm over an FSR with a step of 0.005 nm.

the $(\theta_{h1}, \theta_{q1})$ plane looks like a Lissajous pattern, while that into $(\theta_{h1}, \theta_{h2})$ becomes a spiral. All trajectories have the periodicity of the FSR (0.8 nm), and θ_{q2} is fixed at 67.5° .

To investigate the trend, the loci for various values of θ_{p1} are shown in Fig. 6(a) and 6(b). For variation of θ_{p1} with a fine wavelength-shift step of 0.005 nm, the loci are always obtained, and thus there is no need to delicately align a PMF when splicing, which becomes favorable for implementing the present filter.

III. CHARACTERIZATION OF OPTICAL PROPERTIES

To demonstrate continuous tunability, the filter was constructed using a fiber-pigtailed four-port PBS (OZ OpticsTM), two fiber-pigtailed HWPs (OZ OpticsTM), two fiber-pigtailed QWPs (OZ OpticsTM), and two equal-length bow-tie-type PMF segments (FibercoreTM), as shown in

Fig. 1. A broadband source (BBS) was amplified with a spontaneous emission source (Fiberlabs FL7701TM), and an optical spectrum analyzer (OSA) (Yokogawa AQ6370CTM) was employed to measure the transmission spectra of the filter. The calculated and measured transmission spectra are shown in Figs. 7(a)~7(d) for dip wavelengths of 1548.0, 1548.2, 1548.4, and 1548.6 nm respectively. One can see that the calculated and measured transmission spectra are shifted by 0.2 nm. The insertion loss was measured as 5.87 dB, which originates from the PBS, the butt-coupling of PBS and PMF2, inherent insertion losses of HWPs and QWPs, and fusion splicing of PMFs and single-mode fibers for wave-plate pigtails.

It is often desirable that comb filters have both a flattened pass band and small dispersion in each pass band. To validate the optical properties of the filter, further simulations were carried out. The calculated pass band and its corresponding group-delay time are shown in Fig. 8(a). The 3-dB bandwidth is calculated to be 0.5125 nm, which is larger than that of a zeroth-order comb filter by 0.4 nm [18].

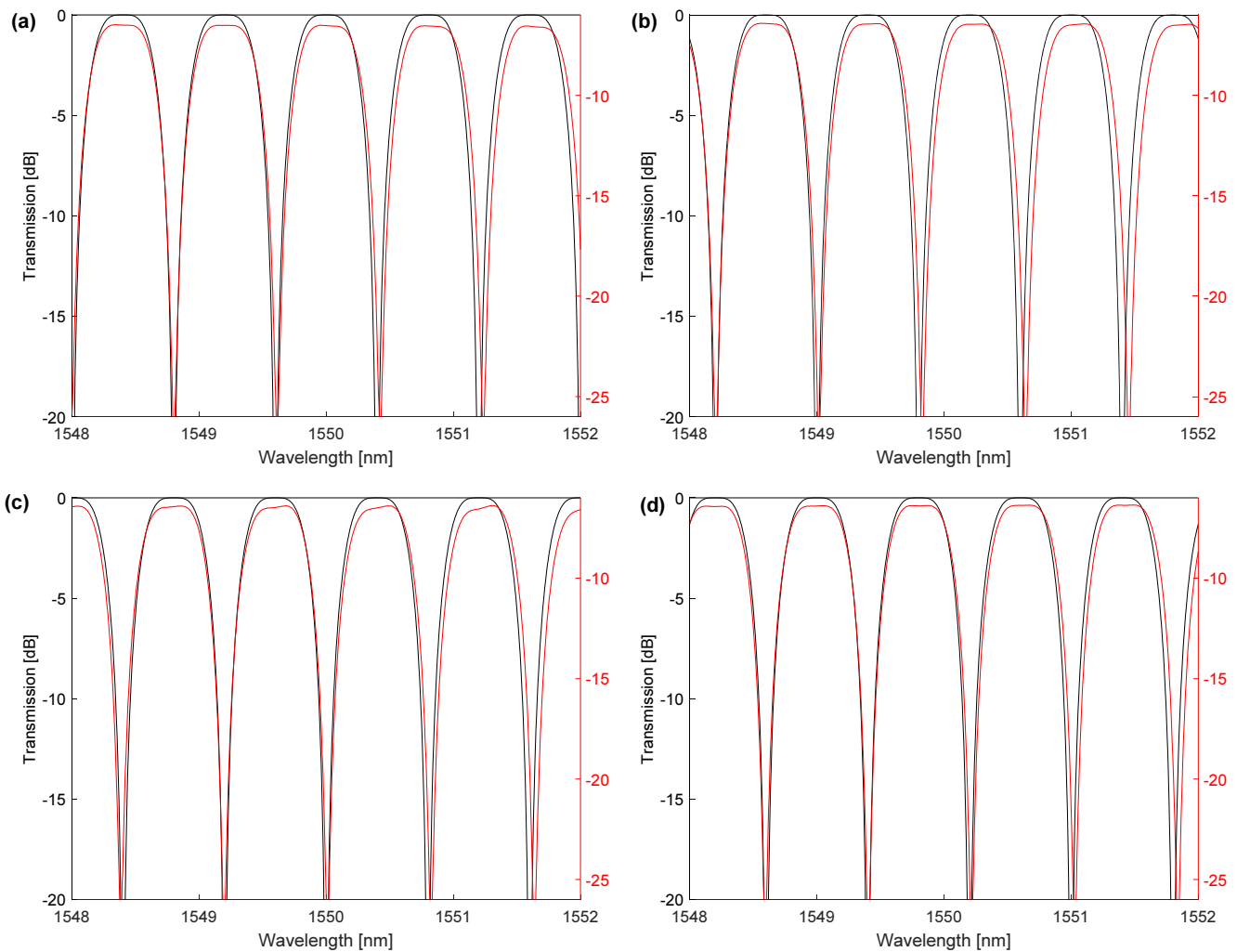


FIG. 7. Calculated (black) and measured (red) wavelength-tuned transmission spectra for various dip wavelengths of (a) 1548.0, (b) 1548.2, (c) 1548.4, and (d) 1548.6 nm.

The dispersion and differential group delay are also essential parameters for designing wavelength-selective filters in optical networks. The group-velocity dispersion is defined as the derivative of the group-delay time with respect to the wavelength, as follows:

$$D = \frac{d\tau_g}{d\lambda} \quad (1)$$

where τ_g is the group-delay time.

The differential group delay (DGD) of a device is defined as the maximum difference in group delay between all polarization states. The calculated group-velocity dispersion and DGD with each maximum value of 15.5 ps/nm and 14.2 ps are shown in Fig. 8(b), which features good characteristics, compared to fiber gratings [23].

We will show in this section that for given orientation angles of the wave plates, the angle combinations that produce the same transmission spectrum can be deduced by the use of the Poincaré sphere. Let us consider an angle locus that covers the whole FSR, and assume that $(\theta_{h1}, \theta_{q1}, \theta_{h2}, \theta_{q2})$ is a point on it. The HWP1 rotates the incident

light by π into a point on the equator making an angle of $4\theta_{h1}$ with respect to the S_1 axis, and thus θ_{h1} has a periodicity of $\pi/2$. Similarly, the HWP2 rotates the SOP circle after PMF1 by π and locates its center at a point that is apart arc distance $4\theta_{h2}$, also implying a periodicity of $\pi/2$. If we assume a new angle set $(\theta_{h1}', \theta_{q1}', \theta_{h2}', \theta_{q2}')$, these relations are expressed as follows:

$$\theta_{h1}' = \theta_{h1} + \pi/2, \quad \theta_{h2}' = \theta_{h2} + \pi/2. \quad (2)$$

The S_1 - S_2 projection planes from the Poincaré sphere for multiple angle sets in a locus that result in the same transmission spectrum through the combination of the respective optical elements are depicted in Fig. 9. Suppose that point A represents the SOP after QWP1, as shown in Fig. 9(a). If $\theta_{q1}' = \theta_{q1} + \pi/2$, the condition for the new SOP after QWP1 to reach point A is such that $4\theta_{h1}'$ is symmetric to $4\theta_{h1}$ with respect to $2\theta_{q1}$; that is, $\theta_{h1}' = -\theta_{h1} + \theta_{q1}$, as shown in Fig. 9(a).

Meanwhile, let us consider another case for the combination of HWP1, QWP1, PMF1, HWP2, and QWP2. In Fig. 9(b), if $4\theta_{h1}'$ and $4\theta_{h2}'$ are symmetric to $4\theta_{h1}$ and $4\theta_{h2}$

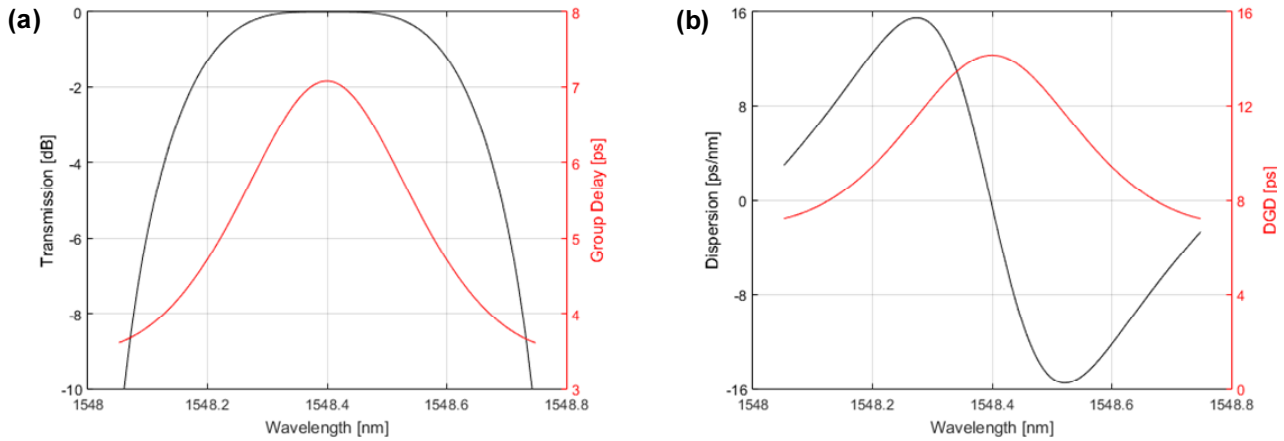


FIG. 8. (a) Calculated pass band and group-delay response, (b) group-velocity dispersion and DGD over an FSR.

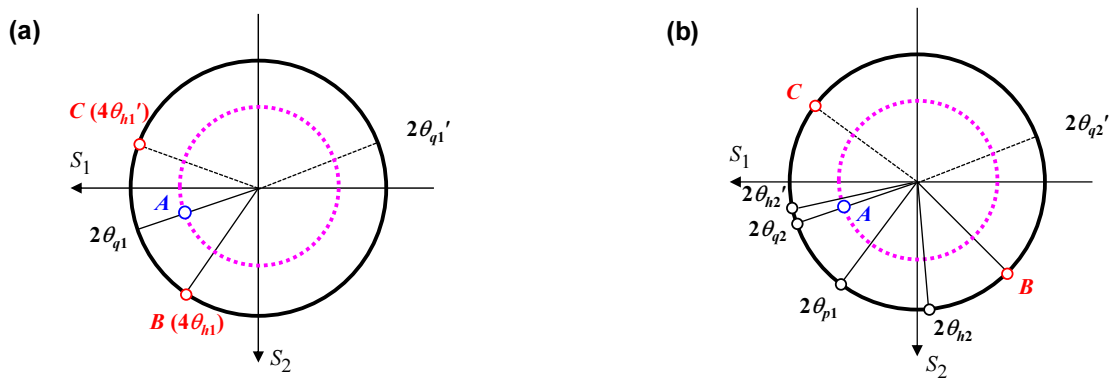


FIG. 9. (a) QWP1 and HWP1 and (b) QWP1, HWP1, PMF1, QWP2, and HWP2 combinations. S_1 - S_2 projection planes from the Poincaré sphere for multiple angle sets in the locus are depicted. The degeneracies are observed with respect to the combination of optical elements within the PDLC.

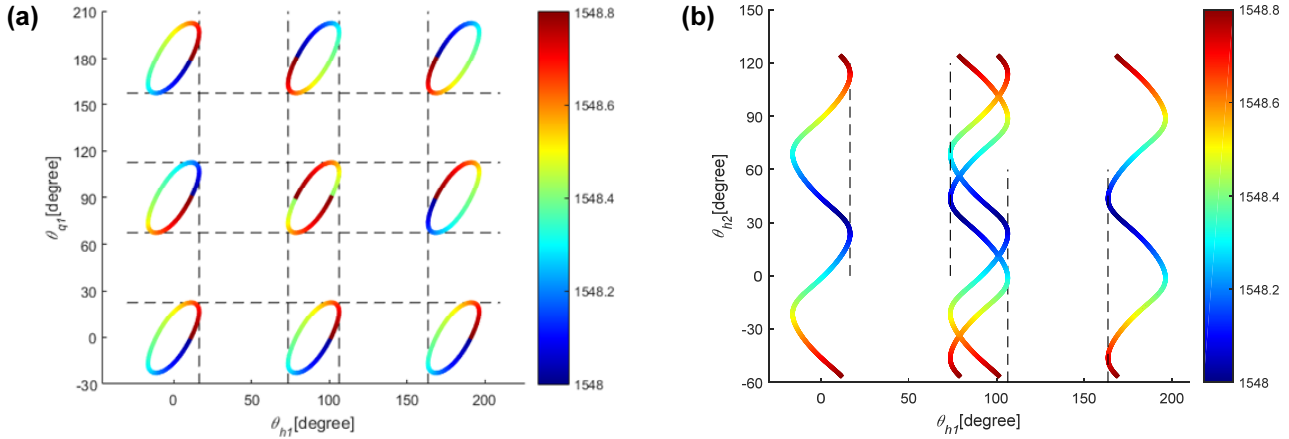


FIG. 10. Periodicity of wave-plate angle loci produced by degeneracies through combinations of optical elements within the PDLC, for (a) $(\theta_{h1}, \theta_{q1})$ and (b) $(\theta_{h1}, \theta_{q2})$.

with respect to $2\theta_{p1}$, and $\theta_{q2}' = \theta_{q2} + \pi/2$, the new angles are as follows:

$$\theta_{h1}' = -\theta_{h1} + \theta_{p1}, \quad \theta_{q1}' = -\theta_{q1} + 2\theta_{p1}, \quad \text{and} \quad \theta_{q2}' = \theta_{q2} + \pi/2. \quad (3)$$

Suppose that B and C represent the centers of circular SOPs after QWP2, whose azimuthal angles are $4\theta_{h2} - 2\theta_{p1}$ and $4\theta_{h2}' - 2\theta_{p1}$ respectively. For the same circular SOP after QWP2, B and C must be symmetric with respect to QWP2, and thus the relation for the orientation angles of HWP2 and the other elements is as follows:

$$\theta_{h2}' = -\theta_{h2} + \theta_{q2} + \theta_{p1}. \quad (4)$$

The multiple loci obtained as explained earlier are shown in Figs. 10(a) and 10(b) for $(\theta_{h1}, \theta_{q1})$ and $(\theta_{h1}, \theta_{h2})$ respectively. Periodic gaps occur and are calculated to be θ_{h1} , θ_{q1} , and θ_{h2} ($\Delta\theta_{h1}$, $\Delta\theta_{q1}$, $\Delta\theta_{h2}$) as 57.2° , 45° , and 57.2° respectively. It is noteworthy that the locus at the center of the $(\theta_{h1}, \theta_{q1})$ figure consists of two opposite directional traces that are rotating CW and CCW.

IV. CONCLUSION

We characterize the optical properties of a tunable pass-band-flattened fiber comb filter based on the PDLC, using the Poincaré-sphere representation. The flatness of the pass band is checked quantitatively in the design process by visualization of the SOP through a world map. The working principle of the filter is described, and tuning performance is verified experimentally. The pass-band-shape-design and wavelength-tuning algorithms are presented in detail. The orientation-angle loci of the wave plates, and their periodicities through the combination of the respective optical elements, are deduced using a geometrical method via the Poincaré sphere. The optical characteristics are investigated, including transmission, group-velocity dispersion,

and DGD. It is found that the 3-dB bandwidth, maximum dispersion, and DGD of the filter are respectively 0.5125 nm, 15.5 ps/nm, and 14.2 ps over the FSR of 0.8 nm. The characterization in this work provides a qualitative understanding of the optical properties of the fiber comb filter based on the PDLC, and this filter may find significant applications in multiwavelength optical systems.

ACKNOWLEDGMENT

This research was supported by a grant from the Marine Biotechnology Program (20150220) funded by the Ministry of Oceans and Fisheries, Korea.

REFERENCES

1. X. T. Hasegawa, K. Inoue, and K. Oda, "Polarization independent frequency conversion by fiber four-wave mixing with a polarization-diversity technique," *IEEE Photon. Technol. Lett.* **5**, 947-949 (1993).
2. S. Roh, S. Chung, Y. W. Lee, I. Yoon, and B. Lee, "Channel-spacing and wavelength-tunable multiwavelength fiber ring laser using semiconductor optical amplifier," *IEEE Photon. Technol. Lett.* **18**, 2302-2304 (2006).
3. I. Yoon, Y. W. Lee, J. Jung, and B. Lee, "Tunable multiwavelength fiber laser employing a comb filter based on a polarization-diversity loop configuration," *J. Lightw. Technol.* **24**, 1805-1811 (2006).
4. Z.-C. Luo, W.-J. Cao, A.-P. Luo, and W.-C. Xu, "Polarization-independent, multifunctional all-fiber comb filter using variable ratio coupler-based Mach-Zehnder interferometer," *J. Lightw. Technol.* **30**, 1857-1862 (2012).
5. Z.-C. Luo, A.-P. Luo, W.-C. Xu, H.-S. Yin, J.-R. Liu, Q. Ye, and Z.-J. Fang, "Tunable multiwavelength passively mode-locked fiber ring laser using intracavity birefringence-induced comb filter," *IEEE Photon. J.* **2**, 571-577 (2010).
6. H.-Y. Jiang, L.-S. Yan, J. Ye, W. Pan, B. Luo, and X.-H.

- Zou, "Polarization-diversified photonic comb filter with independently tunable free spectrum range," *Opt. Lett.* **39**, 4970-4973 (2014).
7. L. R. Chen, "Tunable multiwavelength fiber ring lasers using a programmable high-birefringence fiber loop mirror," *IEEE Photon. Technol. Lett.* **16**, 410-412 (2004).
 8. C. S. Kim and J. U. Kang, "Multiwavelength switching of Raman fiber ring laser incorporating composite polarization maintaining fiber Lyot-Sagnac filter," *Appl. Opt.* **43**, 3151-3157 (2004).
 9. C. S. Kim and J. U. Kang, "Polarization-independent "Figure-Eight" birefringent Sagnac variable comb-filter/attenuator," *IEEE Photon. Technol. Lett.* **16**, 494-496 (2004).
 10. M. P. Fok, K. L. Lee, and C. Shu, "Waveband-switchable SOA ring laser constructed with a phase modulator loop mirror filter," *IEEE Photon. Technol. Lett.* **17**, 1393-1395 (2005).
 11. Y. G. Han, G. Kim, J. H. Lee, S. H. Kim, and S. B. Lee, "Lasing wavelength and spacing switchable multiwavelength fiber laser from 1510 to 1620 nm," *IEEE Photon. Technol. Lett.* **17**, 989-991 (2005).
 12. G. Sun, D. S. Moon, A. Lin, W. T. Han, and Y. Chung, "Tunable multiwavelength fiber laser using a comb filter based on erbium-ytterbium co-doped polarization maintaining fiber loop mirror," *Opt. Express* **16**, 3652-3658 (2008).
 13. A.-P. Luo, Z.-C. Luo, W.-C. Xu, and H. Cui, "Wavelength switchable flat-top all-fiber comb filter based on a double-loop Mach-Zehnder interferometer," *Opt. Express* **18**, 6056-6063 (2010).
 14. J.-J. Guo, Y. Yang, and G.-D. Peng, "Analysis of polarization-independent tunable optical comb filter by cascading MZI and phase modulating Sagnac loop," *Opt. Commun.* **284**, 5144-5147 (2011).
 15. Y. Zhao, T.-T. Song, and Z.-W. Huo, "Tunable optical fiber filter based on a fiber Bragg grating loop mirror," *J. Lightw. Technol.* **29**, 3672-3675 (2011).
 16. X. Liu, L. Zhan, S. Luo, Y. Wang, and Q. Shen, "Individually switchable and widely tunable multiwavelength erbium-doped fiber laser based on cascaded mismatching longperiod fiber gratings," *J. Lightw. Technol.* **29**, 3319-3326 (2011).
 17. Y. W. Lee, K. J. Han, J. Jung, and B. Lee, "Polarization-independent tunable fiber comb filter," *IEEE Photon. Technol. Lett.* **16**, 2066-2068 (2004).
 18. J. Jung and Y. W. Lee, "Tunable fiber comb filter based on simple waveplate combination and polarization-diversified loop," *Opt. Laser Technol.* **91**, 63-70 (2017).
 19. Y. W. Lee, J. Jung, B. Lee, "Wavelength-switchable flat-top fiber comb filter based on a Solc type birefringence combination," *Opt. Express* **13**, 1039-1048 (2005).
 20. S. Jo, Y. Kim, and Y. W. Lee, "Study on transmission and output polarization characteristics of a first-order Lyot-type fiber comb filter using polarization-diversity loop," *IEEE Photon. J.* **7**, 7801015 (2015).
 21. J. Jung and Y. W. Lee, "Continuously wavelength-tunable passband-flattened fiber comb filter based on polarization-diversified loop structure," *Sci. Rep.* **7**, 8311 (2017).
 22. Y. W. Lee and J. Jung, "Simplified tunable fiber comb filter based on polarization-diversity loop configuration," *Opt. Eng.* **56**, 026113 (2017).
 23. C. Lee, R. Lee, and Y. Kao, "Design of multichannel DWDM fiber Bragg grating filters by Lagrange multiplier constrained optimization," *Opt. Express* **14**, 11002-11011 (2006).